Long-term Evolution of Tightly-Packed Stellar Black Holes in AGN Disks: Formation of Merging Black-Hole Binaries via Close Encounters

Jiaru Li , ¹ Dong Lai , ¹ and Laetitia Rodet ¹

¹ Center for Astrophysics and Planetary Science, Department of Astronomy, Cornell University, Ithaca, NY 14853, USA

Submitted to ApJ

ABSTRACT

We study the long-term evolution of two or more stellar black holes (BHs) on initially separated but unstable circular orbits around a supermassive BH (SMBH). Such a close-packed orbital configuration can naturally arise from BH migrations in the AGN disk. Dynamical instability of the orbits leads to recurring close encounters between two BHs, during which the BH separation $r_{\rm p}$ becomes less than the Hill radius $R_{\rm H}$. In the rare very close encounters (with $r_{\rm p}$ several orders of magnitude less than $R_{\rm H}$), a tight merging BH binary can form with the help of gravitational wave emission. We use N-body simulations to study the time evolution of close encounters of various degrees of "closeness" and the property of the resulting binary BH mergers. For a typical "SMBH + 2 BHs" system, the averaged cumulative number of close encounters (with $r_{\rm p} \lesssim R_{\rm H}$) scales approximately as $\propto t^{0.5}$. The minimum encounter separation $r_{\rm p}$ follows a linear cumulative distribution $P(\langle r_{\rm p} \rangle \propto r_{\rm p})$ for $r_{\rm p} \ll R_{\rm H}$. From these, we obtain a semi-analytical expression for the averaged rate of binary captures that lead to BH mergers. Our results suggest that close-packed BHs in AGN disks may take a long time $(\geq 10^7)$ orbits around the SMBH) to experience a sufficiently close encounter and form a bound binary, although this time can be shorter if the initial BH orbits are highly aligned. The BH binary mergers produced in this scenario always have high eccentricities when entering the LIGO band, and have a broad distribution of orbital inclinations relative to the original AGN disk. We also explore the effects of the gas disk and find that simple gas drags on the BHs do not necessarily lead to an enhanced BH binary capture rate.

Keywords: Active galactic nuclei(16); Black holes(162); Galaxy accretion disks(562); Gravitational wave sources(677); N-body simulations(1083)

1. INTRODUCTION

Binary black hole (BBH) mergers are the most common sources of gravitational waves (GWs) detected by the LIGO/Virgo collaboration (Abbott et al. 2019, 2021; The LIGO Scientific Collaboration et al. 2021). A variety of formation channels for these merging BBHs have been studied, ranging from isolated binary evolution (e.g., Lipunov et al. 1997; Podsiadlowski et al. 2003; Belczynski et al. 2010, 2016; Mandel & de Mink 2016; Marchant et al. 2016), strong gravitational scatterings in dense star clusters (e.g., Portegies Zwart & McMillan 2000; O'Leary et al. 2006; Miller & Lauburg 2009; Banerjee et al. 2010; Downing et al. 2010; Ziosi et al.

Corresponding author: Jiaru Li jiaru Li@astro.cornell.edu

2014; Samsing et al. 2014; Rodriguez et al. 2015; Samsing & D'Orazio 2018; Kremer et al. 2019), and tertiary-induced mergers in stellar triple/quadrupole systems (e.g., Miller & Hamilton 2002; Silsbee & Tremaine 2017; Liu & Lai 2018, 2019; Liu et al. 2019a; Fragione & Kocsis 2019) or in nuclear clusters around a central supermassive BHs (e.g., Antonini & Perets 2012; VanLandingham et al. 2016; Petrovich & Antonini 2017; Hamers et al. 2018; Liu et al. 2019b; Liu & Lai 2021). The probability and significance of each channel are still unclear.

The possibility of BBH mergers in AGN accretion disks around supermassive black holes (SMBHs) has received much attention in recent years (e.g., McKernan et al. 2012, 2014; Bartos et al. 2017; Stone et al. 2017; Secunda et al. 2019, 2020; Yang et al. 2019a,b; Gröbner et al. 2020; Ishibashi & Gröbner 2020; Tagawa et al. 2020a,b; Ford & McKernan 2021). BBHs in flat disks

may be hardened, or even driven to merger, by a series of nearly co-planar binary-single scatterings (e.g., Stone et al. 2017; Leigh et al. 2018; Samsing et al. 2020). Hydrodynamical interaction between the gaseous AGN disk and a pre-existing BH binary may also influence the orbital evolution of the binary (Baruteau et al. 2011; Li et al. 2021a,b; Li & Lai 2022). BH Mergers that happen inside AGN disks could have several observable properties, such as the possible associations with electromagnetic counterparts (Stone et al. 2017; McKernan et al. 2019; Graham et al. 2020) and distinct mass and spin distributions (e.g., McKernan et al. 2018; Yang et al. 2019a).

The AGN disk channel of BBH mergers typically relies on the disks being an ideal environment for dynamical formation of BH binaries. BBHs could be "pre-existing" in nuclear star clusters and get captured in the inner AGN disks (Bartos et al. 2017) or form in situ in the extended region of the disks (Stone et al. 2017). It was suggested that AGN disks (Sirko & Goodman 2003; Thompson et al. 2005) may contain migration traps where stellar-mass BHs (sBHs) can accumulate (Bellovary et al. 2016). Orbiters inside such traps can have close encounters with each other due to their mutual gravity and potentially form binaries (Secunda et al. 2019, 2020). A direct gas-capture channel has also been proposed to form binaries from single sBHs (Tagawa et al. 2020b).

An important and unsolved issue of the AGN disk BBH merger scenario is the evolution of sBHs during close encounters and how bound BBHs actually form. Previous studies tend to adopt very simple prescriptions for BBH formation and follow-up evolution. For example, Secunda et al. (2019) performed N-body simulations of multiple sBHs and included disk force prescriptions to mimic the effects of eccentricity damping and migration traps, but they assumed that all close encounters between two BHs within the mutual Hill radius and with negative relative binary energy lead to the formation of bound binaries that quickly merge. This assumption is problematic as the vast majority of such bound binaries are short-lived and are quickly destroyed by the tidal force of the SMBH. Tagawa et al. (2020b) considered gas-assisted binary formation in their population synthesis study, including the time delay between BBH formation and merger, and allowing newly formed BBHs to be disrupted before mergers. However, their studies are one-dimensional and they assumed that the relative orbits of all BBHs are circular for simplicity.

In this paper, we study how often two or more sBHs in closely-packed, initially circular and nearly co-planar orbits around a SMBH can be captured into a "perma-

nent" binary and merge with the aid of the gravitational radiation. Such close-packed orbits (with the difference in orbital radii less than a few times the Hill radius $R_{\rm H}$) can be naturally produced by the differential migrations of sBHs in the AGN disk and/or the migration traps (Bellovary et al. 2016; Secunda et al. 2019). Since the sBHs in close orbits are dynamically unstable, they exhibit chaotic orbital motion around the SBMH and undergo repeated close encounters with each other (with their separation less than $R_{\rm H}$). Binary capture occurs only in the very rare occasion when two sBHs experience an extreme close encounter (with their separation several orders of magnitude less than $R_{\rm H}$), during which energy dissipation through GW emission is effective. We perform a large number of N-body simulations to study the occurrence rate of such close encounters and the properties of the captured BBHs. Since the dynamical influence of the disk gas on sBHs during close encounters is highly uncertain, the major part of our paper focuses on the clean problem where the only dissipative effect is GW emission. Nevertheless, we also carry out an exploratory study on the gas effects by adding "frictional" forces on the sBHs to mimic the BH-gas interactions.

The rest of this paper is structured as follows. Section 2, we introduce our scenario for BBH formation in AGN disks via close encounters between sBHs. In Section 3, we describe our fiducial "SMBH + 2 BHs" simulations with no gas effects included. We use these simulations to obtain the time evolution of the close encounter rate, the distribution of the minimum sBH separations during encounters, and the timescale (and the probability) to form long-lived or merging BH binaries. Section 4 discusses how our results depend on the initial inclinations of the BH orbits around the SMBH. In Section 5 we apply simple models of the disk forces on the sBHs to assess the effects of gas disks on the evolution of the embedded sBHs and the formation rate of merging BBHs. Section 6 explores the rate and properties of the close encounters in systems with more than two sBHs around the SMBH. In Section 7, we summarize our findings.

2. SCENARIO

AGN disks can help bringing stellar-mass black holes (sBHs) circulating around a supermassive BH (SMBH) into close orbits due to the differential migrations of the BHs and migration traps (Bellovary et al. 2016), therefore promoting close encounters between the sBHs. While the encountering sBHs typically have too much relative kinetic energy to become bound in the presence of the tidal field of the SMBH, they may occasionally have a very close encounter, during which gravitational

wave (GW) emission can take away the excessive energy. Dynamical friction from the disk gas may also play a role, but its effect is more difficult to quantify. These very close encounters may turn the two BHs into a bound binary and lead to BBH merger.

We consider a system with a central SMBH of mass M, around which orbit two or more sBHs on nearly circular and nearly co-planar trajectories. For simplicity, henceforth 'BHs' always refer to stellar-mass black holes that are orbiting around the SMBH. Due to their migrations in the AGN disk, the BHs may have orbits very close to each other. For the most part of this paper, we set up two BHs with masses m_1 , m_2 and initial semi-major axes a_1 , a_2 around the SMBH. If the dimensionless orbital separation (in units of the mutual Hill radius $R_{\rm H12}$) is less than a critial value, i.e.

$$\frac{a_2 - a_1}{R_{\rm H12}} \equiv K < K_{\rm crit} \sim 1,$$
 (1)

where

$$R_{\rm H12} \equiv \frac{a_1 + a_2}{2} \left(\frac{m_1 + m_2}{3M}\right)^{1/3},$$
 (2)

the orbits are dynamically unstable, such that the two BHs will soon develop orbital crossing and start chaotic evolution. The boundary between "stable" and "unstable" can be fuzzy but the critical value $K_{\rm crit}$ is of order unity and depends on the "frictional" force acting on the BH from the disk gas (Li, Rodet and Lai 2022). In the absence of BH-disk interaction, the Hill stability criterion gives $K_{\rm crit}=2\sqrt{3}$ (Gladman 1993).

There are three possible outcomes for the two BHs in unstable orbits: (i) The lighter BH (m_2) is ejected from the system; (ii) The two BHs experience a sufficiently close encounter such that GW emission and/or gas drag makes them into a bound binary and eventually merge; (iii) One of the BHs moves very close to the SMBH and gets "swallowed" by it. Outcome (iii) has a negligible probability when $a_1, a_2 \gg GM/c^2$, i.e. when the horizon radius of the SMBH is much less than the BH orbital distances. In our "SMBH + 2 BHs" systems with $M \gg m_1, m_2$, outcome (i) will take many orbital periods to happen. This can be understood as follows. Close encounters between m_1 and m_2 (< m_1) cause m_2 to experience energy diffusion, with the change (loss or gain) of energy during each encounter given by $\Delta E \sim \alpha (Gm_1m_2/a_1)$, where $\alpha \gtrsim 1$. Thus the average number of close encounters required for m_2 to be ejected is $\langle N_{\rm ej} \rangle \sim (GMm_2/2a_1)^2 (\Delta E)^{-2} \sim (4\alpha^2)^{-1} (M/m_1)^2$. Indeed, extensive numerical experiments carried out by Pu & Lai (2021) show that $N_{\rm ej}$ has a broad distribution,

with the mean value given by (see their Eq 24)

$$\langle N_{\rm ej} \rangle \simeq 0.06^2 \left(\frac{M}{m_1}\right)^2 \left(1 + \frac{m_2}{m_1}\right)^4,$$
 (3)

and the distribution has a long tail at the larger values (the 68% quantile of $N_{\rm ej}$ ranges from $0.25 \langle N_{\rm ej} \rangle$ to $13 \langle N_{\rm ej} \rangle$). The ejection time is usually much longer then $N_{\rm ej}P_2$ (where P_2 is the initial orbital period of m_2) since the semi-major axis of m_2 increases as it approaches ejection. Thus, for $M/m_1 \gtrsim 10^6$, the ejection timescale $t_{\rm ej} \gg 10^{10}P_2$, which means ejection almost never happens.

We are thus left with outcome (ii), i.e. BH binary formation due to dissipative processes. If we neglect the possible effect of gas drag, the only dissipation is GW emission ("gravitational bremsstrahlung"). During a very close encounter (i.e. the separation between m_1 and m_2 is much less than $R_{\rm H}$), the two BHs lose their relative energy by the amount (Peters 1964; Quinlan & Shapiro 1989)

$$\Delta E_{\rm GW} = \frac{85\pi}{12\sqrt{2}} \frac{G^{7/2}\mu^2 m_{12}^{5/2}}{c^5 r_{\rm p}^{7/2}},\tag{4}$$

where $m_{12} = m_1 + m_2$, $\mu = m_1 m_2 / m_{12}$, and r_p is the periastron separation of the relative trajectory of the BHs. To form a binary that is stable in the presence of the SMBH tidal field, we require

$$\Delta E_{\rm GW} \gtrsim \eta \frac{Gm_1m_2}{R_{\rm H12}},$$
 (5)

with η of order unity. This implies that the pericenter distance of the relative orbit of m_1 and m_2 must be less than the critical value for capture, given by

$$\begin{split} \frac{r_{\rm cap}}{R_{\rm H12}} &\simeq 2.85 \eta^{-2/7} \left(\frac{\mu}{m_{12}}\right)^{2/7} \left(\frac{m_{12}}{M}\right)^{10/21} \left(\frac{a_{12}}{GM/c^2}\right)^{-5/7}, \\ &\simeq 10^{-4} \eta^{-2/7} \left(\frac{4\mu}{m_{12}}\right)^{2/7} \left(\frac{10^6 m_{12}}{M}\right)^{10/21} \\ &\times \left(\frac{a_{12}}{100GM/c^2}\right)^{-5/7}, \end{split} \tag{6}$$

where $a_{12} = (a_1 + a_2)/2 \simeq a_1$. Thus, for the two unstable BHs to be captured into a bound binary requires an extremely close encounter with $r_{\rm p} \lesssim 10^{-4} R_{\rm H12}$. A major goal of our paper is to evaluate the rate of such extremely close encounters and the properties of the resulted merging BH binaries.

3. FORMATION OF BOUND BINARIES IN "SMBH + 2 BHS" SYSTEMS

In this section, we study the formation rate of bound binaries for two BHs in unstable orbits around a SMBH. We neglect the effects of gas disk (if any) here – these effects will be studied in Section 5.

3.1. Setup of simulations

The fiducial system of our simulations consists of a central SMBH with mass M and two smaller BHs with mass $m_1 = 2 \times 10^{-5} M$ and $m_2 = 10^{-5} M$. The initial orbital separation is set as

$$a_2 - a_1 = 2R_{\rm H12},\tag{7}$$

so that their orbits are unstable. For convenience, henceforth we define

$$R_{\rm H} \equiv a_1 \left(\frac{m_1}{3M}\right)^{1/3} = \left(\frac{m_1}{m_{12}}\right)^{1/3} R_{\rm H12}$$
 (8)

to be the Hill radius of the m_1 at the beginning of the simulation and use it as the unit of distance. We let P_1 be the initial orbital period of m_1 and use it as the unit of time. We note that P_1 at $a_1 = 100GM/c^2$ for $M = 10^6 M_{\odot}$ is 10^{-3} yr. The BHs are given initial eccentricities $e_1 = 0$, $e_2 = 10^{-5}$, and inclinations $i_1 = i_2 = R_{\rm H}/a_1$. We carry out 2000 runs and sample the initial values of the argument of the peripasis, the longitude of the ascending node, and the mean anomaly randomly in the range $[0, 2\pi]$ for each BH, assuming they all have uniform distributions.

We simulate the evolution of the system using the N-body code REBOUND (Rein & Liu 2012) with the IAS15 integrator (Rein & Spiegel 2015). Each simulation runs for $10^5 P_1$.

3.2. Close encounters

To characterize encounters with various degrees of "closeness", we designate a close encounter event to be "CE α " when the separation between the BHs, $r_{\rm rel} = |{\bf r}_1 - {\bf r}_2|$, becomes less than $10^{-\alpha}R_{\rm H}$ and numerically keep track of CE0, CE1 and CE2 in each simulation. A CE α event starts when $r_{\rm rel}$ changes from $> 10^{-\alpha}R_{\rm H}$ to $< 10^{-\alpha}R_{\rm H}$, and ends when $r_{\rm rel}$ becomes greater than $10^{-\alpha}R_{\rm H}$ again and the relative energy $E_{\rm rel} = \frac{1}{2}\mu |{\bf v}_1 - {\bf v}_2|^2 - \frac{Gm_1m_2}{r_{\rm rel}}$ is positive. The whole process is regarded as a single CE α event no matter how long it elapses. In the simulation, a new CE α is logged only if the previous one has ended.

The left panels of Figure 1 show the time evolution of the CE0, CE1, and CE2 counts in 200 examples (out of a total of 2000) of our simulations. Because of the stochastic nature of the evolution, the cumulative event count, $N_{\alpha}(t)$, in one simulation can differ significantly from an-

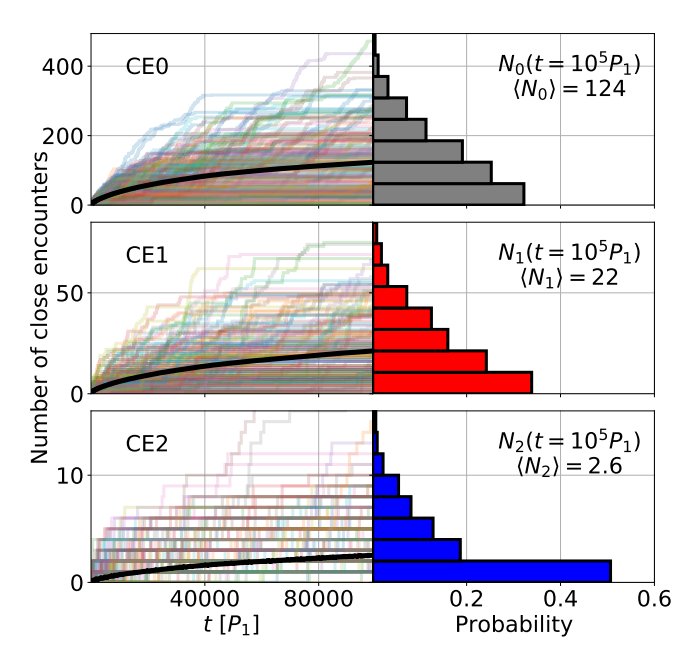


Figure 1. Left: Cumulative number of CE0, CE1 and CE2 events as a function of time for our fiducial "SMBH+2BHs" systems. A CE α event occurs when the separation between the two BHs becomes less than $10^{-\alpha}R_{\rm H}$. In each panel, each of the 200 colored curves represents a simulation of the "SMBH+2BHs" system. The black curve shows the average number of CE α events (averaged over all 2000 runs). Right: Distribution of N_{α} at $t=10^5P_1$ from all simulations. The horizontal axis shows the probability of each bin.

other. The right panel of Figure 1 shows the probability distribution of $N_{\alpha}(t=10^5P_1)$ from all 2000 simulations. The total numbers of CE0, CE1, CE2 events in those simulations are 248790, 43153, 5238, respectively. Thus, at $t=10^5P_1$, the average number per simulation of CE0, CE1, and CE2 are $\langle N_{\alpha}(10^5P_1)\rangle=124,$ 22, and 2.6, respectively. Note that N_{α} has a wide distribution: For example, while $\langle N_2(10^5P_1)\rangle=2.6,$ 5% of the runs have $N_2(10^5P_1)>10$.

Despite the difference in the numbers, the three kinds of CEs all have higher occurrence rate at the early times than at the later times. The time evolution of the average can be described by a power law $\langle N_{\alpha}(t)\rangle \propto t^{n_{\alpha}}$. We perform least-square fits using such power-law to the results at $t\gtrsim 2\times 10^4 P_1$ to exclude the initial transient stage. We find

$$\langle N_0(t)\rangle = 0.67 \left(\frac{t}{P_1}\right)^{0.45},$$
 (9)

$$\langle N_1(t)\rangle = 0.067 \left(\frac{t}{P_1}\right)^{0.50},$$
 (10)

$$\langle N_2(t)\rangle = 0.0064 \left(\frac{t}{P_1}\right)^{0.52}.$$
 (11)

3.3. Very close encounters and BBH formation rate

During each $\text{CE}\alpha$ event, we take a simulation snapshot every $10^{-3}P_1$ and monitor the separation $r_{\text{rel}} = |\boldsymbol{r}_1 - \boldsymbol{r}_2|$ between the two BHs. The exact periapsis passage moment may lie between two of the snapshots. We use the snapshot right after the true pericenter passage (when r_{rel} first increases) to calculate the relative energy and angular momentum of the encountering BHs:

$$E_{\rm rel} = \frac{1}{2} \mu v_{\rm rel}^2 - \frac{G m_1 m_2}{r_{\rm rel}},$$
 (12)

$$\ell_{\rm rel} = r_{\rm rel} \times v_{\rm rel}.$$
 (13)

We then compute the semi-major axis $a_{\rm rel}$ of the orbit via $E_{\rm rel} = -Gm_1m_2/(2a_{\rm rel})$, and the pericenter distance $r_{\rm p}$ using $\ell_{\rm rel} = \sqrt{Gm_{12}a_{\rm rel}(1-e_{\rm rel}^2)} \simeq \sqrt{2Gm_{12}r_{\rm p}}$.

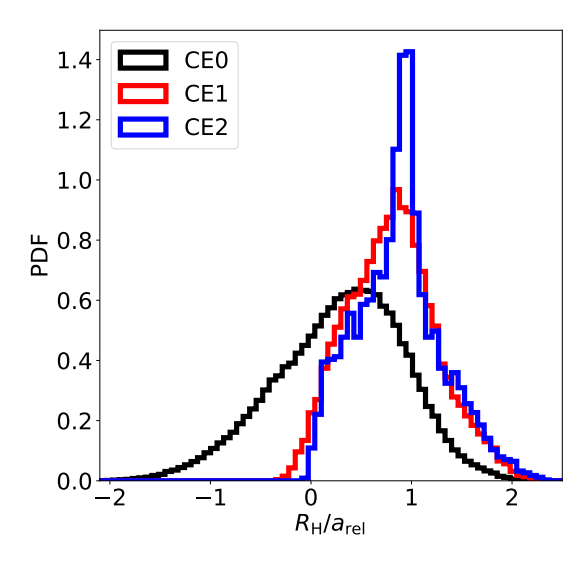


Figure 2. Probability distribution of $R_{\rm H}/a_{\rm rel}$ in our fiducial simulations, where $a_{\rm rel}$ is the semi-major axis of the relative orbit of the BH pairs undergoing close encounters.

Figure 2 shows the distribution of the semi-major axis $a_{\rm rel}$ of the BH binary undergoing close encounters. The most likely $a_{\rm rel}$ is about $R_{\rm H}$, and nearly all close encounters have $R_{\rm H}/a_{\rm rel} \leq 2.3$. Given that the BH pairs during the encounters are either unbound or have $a_{\rm rel} \gtrsim R_{\rm H}$, they quickly depart from each other after reaching their minimum separation and get disrupted by the SMBH tide. This implies that the lifetime of most binaries formed by CEs is less than their orbital period, which is approximately equal to their period around the SMBH when $a_{\rm rel} \sim R_{\rm H}$. Indeed, we find that, among the 248790 CE0 events in our 2000 simulations, the vast majority (96.35%) disentangle within one orbital period (P_1) around the SMBH, and only 0.02% survive for more than $10P_1$.

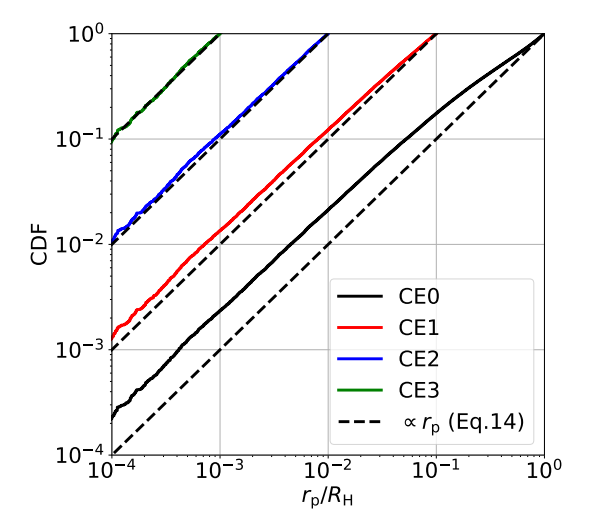


Figure 3. Cumulative distribution of $r_{\rm p}$ in close encounters in our fiducial simulations. The solid colored curves show the distribution normalized for CE0, CE1, CE2 and CE3. The dashed black lines are given by equation (14).

Figure 3 shows the distribution of the pericenter ("closest") distance of the two BHs during close encounters. We find that, for a $\text{CE}\alpha$ event, the cumulative distribution of r_{p} (i.e., the probability for the pericenter distance to be less than r_{p}) is approximately given by

$$P_{\alpha}(< r_{\rm p}) \simeq \frac{r_{\rm p}}{10^{-\alpha}R_{\rm H}}$$
 (for $r_{\rm p} \le 10^{-\alpha}R_{\rm H}$). (14)

Equation (14) becomes increasingly accurate for closer encounters. The difference in $\langle N_{\alpha}(t) \rangle$ for CE0, CE1 and CE2 discussed in Section 3.2 is a direct consequence of this cumulative distribution of $r_{\rm p}$.

Equation (14) is equivalent to a constant probability distribution $dP_{\alpha}/dr_{\rm p}={\rm const.}$ Since the relative angular momentum is $\ell_{\rm rel}\simeq\sqrt{2Gm_{12}r_{\rm p}}$ for nearly parabolic encounters (for $r_{\rm p}\ll a_{\rm rel}\sim R_{\rm H}$; see Figure 2), this is equivalent to the probability distribution in $\ell_{\rm rel}$ given by

$$\frac{dP_{\alpha}}{d\ell_{\rm rel}} \propto \ell_{\rm rel}.\tag{15}$$

This relation has been previously obtained both analytically and numerically in the context of planetary collisions (Li & Lai 2020). It can be understood as follows: When the two BHs reach a close separation $r_{\rm rel} \ll R_{\rm H}$, the angular momentum is $\ell_{\rm rel} = v_{\rm rel} r_{\perp}$, where $v_{\rm rel} \simeq \sqrt{2Gm_{12}/r_{\rm rel}}$ and r_{\perp} is the projection of $r_{\rm rel}$ perpendicular to $v_{\rm rel}$; if the initial mutual inclination of the two BHs is much larger than $r_{\rm rel}/a_1$, the vector r_{\perp} is sampled uniformly in the plane perpendicular to $v_{\rm rel}$ (Li & Lai 2020), i.e. $dP/(r_{\perp}dr_{\perp}) = {\rm const}$, which implies Equation (15).

While Figure 3 depicts the $r_{\rm p}$ -distribution during the whole simulation time span, Figure 4 shows that the CEs from different time intervals also follow to the same distribution.

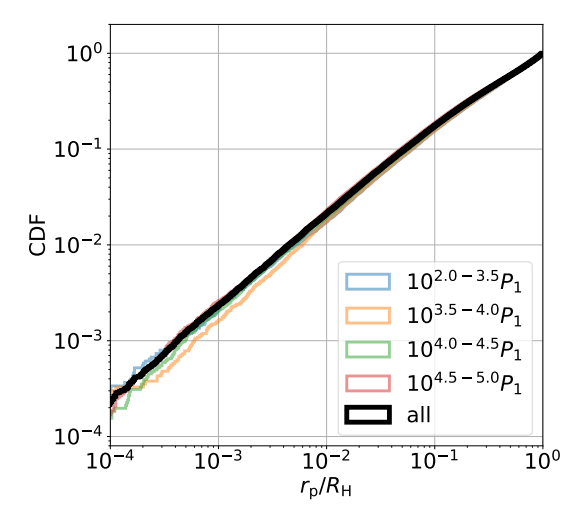


Figure 4. Cumulative distribution of $r_{\rm p}$ in close encounters (CE0s) detected at different time intervals (as labeled) in our fiducial simulations. The black line here is the same as the black line in Figure 3.

Thus, combining Equations (9) and (14), the averaged cumulative number of very close encounters with $r_{\rm p} < r_{\rm cap}$ given by

$$\langle N(t; r_{\rm p} < r_{\rm cap}) \rangle = \langle N_{\alpha}(t) \rangle P_{\alpha}(< r_{\rm cap}).$$
 (16)

Evaluating Equation (16) using $\langle N_2(t) \rangle$ and $P_2(\langle r_{\rm cap})$, we find

$$\langle N(t; r_{\rm p} < r_{\rm cap}) \rangle \simeq 6 \times 10^{-5} \left(\frac{t}{P_{\rm 1}}\right)^{0.52} \times \left(\frac{r_{\rm cap}}{10^{-4}R_{\rm H}}\right),$$
 (17)

where we have scaled $r_{\rm cap}$ according to the estimate given by Equation (6). Thus, for $r_{\rm cap} \simeq 10^{-4} R_{\rm H}$, it would take about $10^8 P_1$ on average for the two BHs to capture into a merging binary by GW emission. Note that, because of the wide spread of N(t) (see Figure 1), it is possible for an unstable pair of BHs to reach $N(t) \simeq 4 \langle N(t) \rangle$ (about 5% of the systems) and be captured in $\sim 10^7 P_1$.

3.4. Orbital obliquities of BH binaries formed in close encounters

The orbital obliquities (i_{bin}) of the BH binaries formed by CEs can be inferred from the inclination of the angular momentum vector ℓ_{rel} of the CE orbits with respect to the initial orbital axis (\hat{z}) around the SMBH,

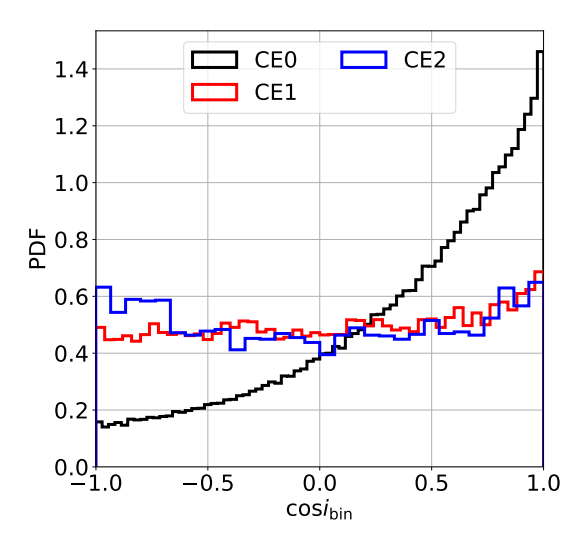


Figure 5. Probability density function of the binary obliquity i_{bin} of BHs in close encounters. Note that i_{bin} measures the angle between the close encounter plane and the orbital plane around the SMBH, i.e. $\cos i_{\text{bin}} \equiv \hat{\ell}_{\text{rel}} \cdot \hat{z}$, where $\hat{\ell}_{\text{rel}}$ is the relative angular momentum axis of the two BHs, and \hat{z} is the initial orbital axis around the SMBH.

i.e. $\cos i_{\rm bin} = \hat{\ell}_{\rm rel} \cdot \hat{z}$. Figure 5 shows the distribution of $\cos i_{\rm bin}$ for the close encounters in our fiducial simulations. Encounters within Hill radius (CE0, black) are predominantly prograde with the most probable $i_{\rm bin}$ being zero. But closer encounters (CE1 and CE2) have nearly uniform distribution of $\cos i_{\rm bin}$. This indicates that merging BH binaries formed in very close encounters ($r_{\rm p} \ll R_{\rm H}$) have a broad range of inclinations with respect to the AGN disk plane.

The broad distribution of $\cos i_{\rm bin}$ is consistent with the findings of Li & Lai (2020) in the context of planet collisions. Such a broad distribution arises when the initial mutual inclination of the BH orbits Δi is much larger than $r_{\rm p}/a_{\rm l}$. Since our simulations have $\Delta i \sim R_{\rm H}/a_{\rm l}$, all CEs with $r_{\rm p} \ll R_{\rm H}$ will have a broad $\cos i_{\rm bin}$ distribution. ¹

3.5. Mass dependence of the close encounter rate

The mass ratio between the SMBH and the BHs in AGN disks can span several orders of magnitude. We repeat our fiducial experiment (which has $m_1=2m_2=2\times 10^{-5}M$) with four different sets of BH masses: $(m_1,m_2)=(8,4)\times 10^{-5}M, (m_1,m_2)=(2,1)\times 10^{-6}M, (m_1,m_2)=(2,1.5)\times 10^{-5}M$. We use them to test the effect of having larger

 $^{^1}$ Li & Lai (2020) showed that when $\Delta i \gg r_{\rm p}/a_1$ and $\Delta i \ll R_{\rm H}/a_1,$ the distribution of $\cos i_{\rm bin}$ is $f(\cos i_{\rm bin}) \propto (1-\cos^2 i_{\rm bin})^{-1/2},$ and that when $\Delta i \gg r_{\rm p}/a_1$ and $\Delta i \sim R_{\rm H}/a_1,~f(\cos i_{\rm bin})$ becomes more uniform.

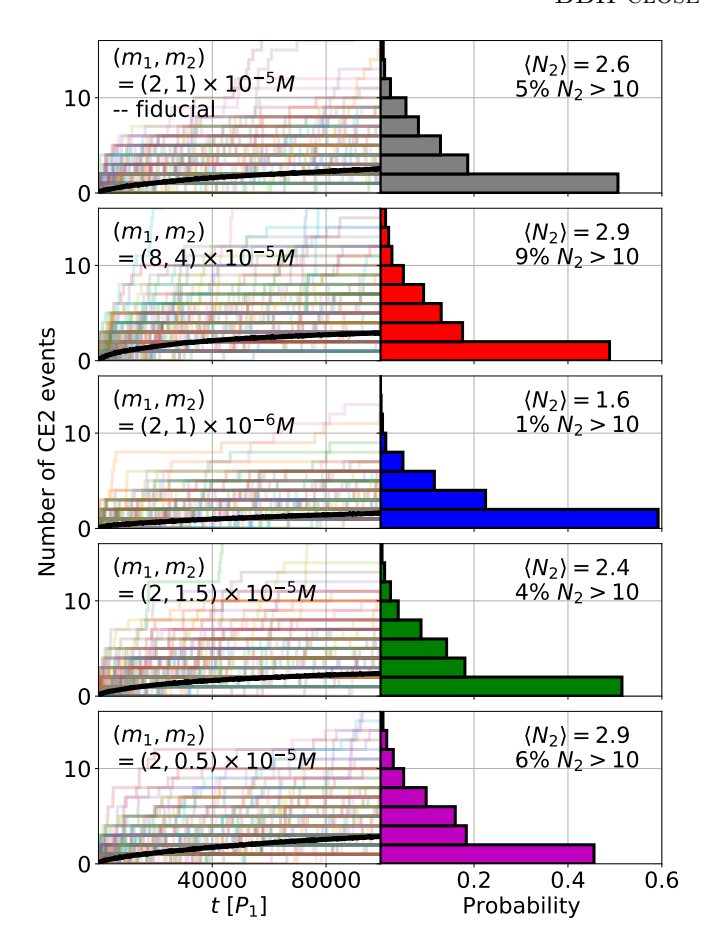


Figure 6. Same as Figure 1, except showing the number of CE2 events in the systems with different BHs masses (as labeled). The texts on the right panels show the average number of N_2 at $t = 10^5 P_1$ and the percentage of the runs that experience more than 10 CE2 events.

BH mass, smaller BH mass, smaller BH mass ratio $(m_1/m_2=4/3)$, and larger BH mass ratio $(m_1/m_2=4)$, respectively.

Figure 6 compares the CE2 event rates in the fiducial system and in the four systems with different BH masses. In all cases, the N_2 -distributions at $t=10^5 P_1$ show large spreads, with the mean $\langle N_2(t=10^5 P_1) \rangle$ in the range of 1.6-2.9 (see Figure 6). The probabilities for high N_2 s (beyond the mean) are more different: for example, the probability for each simulation to get more than 10 CE2 events is 5%, 9%, 1%, 4%, and 6% for the five cases displayed in Figure 6.

We find that, for four systems with different BH masses, the probability distributions of $R_{\rm H}/a_{\rm rel}$, $r_{\rm p}/R_{\rm H}$ and $i_{\rm bin}$ are all similar to the fiducial results as depicted in Figures 2, 3 and 5.

Overall, our results suggest that the BBH formation rate obtained for our fiducial system in Section 3.3 can be applied to other systems with different BH masses (as long as $m_1, m_2 \ll M$) to within a factor of 2. The biggest effect that we observe is a drop in the CE2 rate by a factor of 2 when the BH masses are lowered by a factor of 10 compared to the fiducial system.

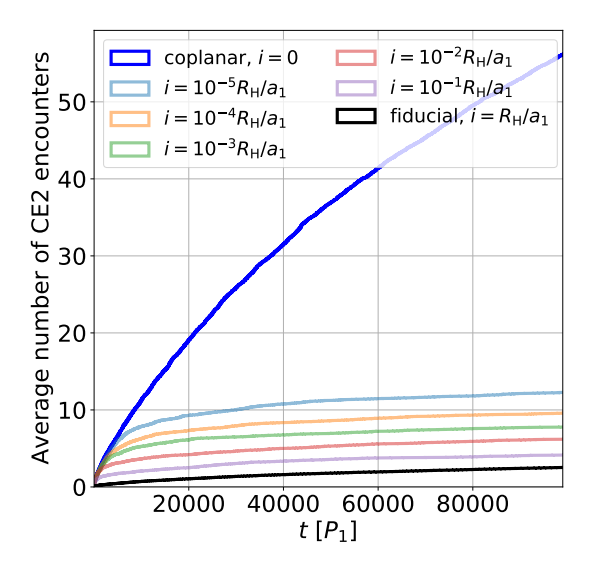


Figure 7. Average number of CE2 events as a function of time in systems with different initial orbital inclinations $(i_1 = i_2 = i$ as labeled). The black curve is the same as the black curve in the bottom left panel of Figure 1.

4. SYSTEMS OF DIFFERENT INITIAL INCLINATIONS

4.1. Results with different initial inclinations

Our simulations in Section 3 assume that the initial orbits of the two BHs have inclinations $i_1=i_2=R_{\rm H}/a_1$ and random longitudes of ascending nodes. We expect the CE rates to increase when i_1 and i_2 are smaller. Figure 7 shows the cumulative number of CE2 counts (averaged over 2000 runs) in simulations with different initial values of i_1 and i_2 . We see that, as expected, $\langle N_2(t) \rangle$ increase as i_1 and i_2 decrease. This increase is highly substantial in the exact coplanar systems ($i_1=i_2=0$), for which we find an average of 56 CE2s at $t=10^5P_1$ and the CE2 rate evolve in time as

$$\langle N_2(t) \rangle \simeq 0.05 \left(\frac{t}{P_1}\right)^{0.61}$$
 (exact coplanar). (18)

This should be compared to Equation (11) for our fiducial runs (which assume $i_1 = i_2 = R_{\rm H}/a_1$). We notice that a smaller (but non-zero) initial inclination leads to more CE2 at the beginning, but the various $\langle N_2(t) \rangle$ curves become roughly parallel after a few ten-thousand orbits, indicating that the rate $d\langle N_2 \rangle/dt$ "saturates" to the fiducial value (see below).

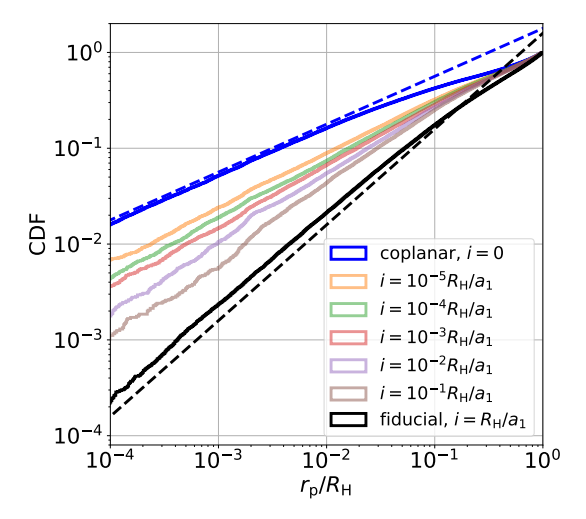


Figure 8. Same as Figure 3, but showing results for the CE0 events only and for different values of the initial orbital inclinations $(i_1 = i_2 = i)$ as indicated by the labels. The black solid curve is the same as in Figure 3. The black dashed line shows the linear $\propto r_{\rm p}$ scaling (see Equation 14) and the blue dashed line shows the $\sqrt{r_{\rm p}}$ scaling (see Equation 19).

The distributions of the pericenter ("closest") distance $r_{\rm p}$ of CE2 for the simulations with different initial inclinations are shown in Figure 8. For the exact co-planar systems, we find that the cumulative distribution of $r_{\rm p}$ is

$$P_{\alpha}(< r_{\rm p}) \simeq \left(\frac{r_{\rm p}}{10^{-\alpha}R_{\rm H}}\right)^{1/2} \quad (\text{for } r_{\rm p} \le 10^{-\alpha}R_{\rm H})(19)$$

This should be contrasted with Equation (14) for our fiducial simulations. Equation (19) is equivalent to a uniform distribution of angular momentum, $dP/d\ell_{\rm rel} = {\rm const.}$ Such a uniform distribution is expected because for $i_1 = i_2 = 0$, the dynamics is confined to the original orbital plane, and at $r_{\rm rel} \ll R_{\rm H}$ the projected separation r_{\perp} is restricted to a line with $dP/dr_{\perp} = {\rm const.}$

Combining Equations (18) and (19), we find that for the exact co-planar systems, the cumulative BH binary formation rate in very close encounters is

$$\langle N(t; r_{\rm p} < r_{\rm cap}) \rangle \simeq 0.005 \left(\frac{t}{P_{\rm 1}}\right)^{0.61} \left(\frac{r_{\rm cap}}{10^{-4}R_{\rm H}}\right)^{1/2} (20)$$

It would only take about $6 \times 10^3 P_1$ on average for the two BHs to form a merging binary. Compared to Equation (17), we see that for such perfectly coplanar systems, the BH binary formation rate is much higher than our fiducial systems (with $i_1 = i_2 = R_{\rm H}/a_1$).

All of the other small initial inclination simulations yield between 0.1 and 1.0 critical CEs with $r_{\rm p} < 10^{-4} R_{\rm H}$ on average in their first $10^5 P_{\rm l}$. We expect their rates to be similar to the fiducial rates over longer timescales (see below).

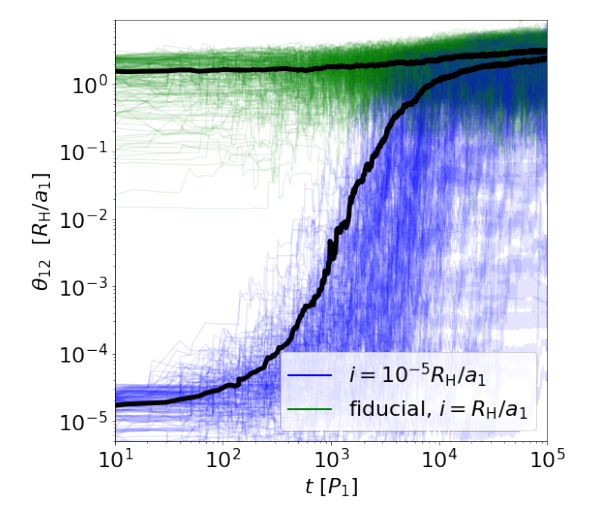


Figure 9. Time evolution of the mutual inclination of the two BH orbits in the fiducial system (green) and in the nearly coplanar system with initial $i_1 = i_2 = 10^{-5} R_{\rm H}/a_1$ (blue). The colored lines represent 200 individual simulations for each system. The black curves represent their averages.

4.2. Evolution of nearly coplanar systems

Figures 7 and 8 show that for nearly coplanar systems (with initial inclinations $0 < i_1, i_2 \ll R_{\rm H}/a_1$), both the cumulative CE2 rate and the $r_{\rm p}$ distribution $P_{\alpha}(< r_{\rm p})$ lie between those of the exact coplanar system and our fiducial system. However, Figure 7 also indicates that while the cumulative number of CE2 events in the first $\sim 10^4$ orbits is much larger than the fiducial case, the rate $d \langle N_2 \rangle / dt$ seems to settle down to the fiducial rate at later times. This suggests that the mutual inclinations of the BH orbits grow in time in systems with nearly coplanar initial orbits.

Figure 9 shows the evolution of mutual inclination θ_{12} of the BH orbits for our fiducial systems and for a system with initial $i_1 = i_2 = 10^{-5} R_{\rm H}/a_1$. The mutual inclination is computed from $\cos\theta_{12} = \hat{\ell}_1 \cdot \hat{\ell}_2$, where $\hat{\ell}_1$ and $\hat{\ell}_2$ are the unit angular momentum vectors of m_1 and m_2 around the SMBH. We see that in the nearly coplanar system, the mutual inclination θ_{12} gradually increases and then saturates at $\theta_{12} \sim R_{\rm H}/a_1$. For our fiducial system, the average mutual inclination remains at $\sim R_{\rm H}/a$ throughout the simulation.

Due to the time evolution of the mutual inclination θ_{12} , we expect that the CE statistics, such as the $r_{\rm p}$ -distribution, also evolve with time in the nearly coplanar systems. Figure 10 shows the time dependence of the $r_{\rm p}$ -distribution for the $i_1=i_2=10^{-5}$ system. It is clear that the initial small inclinations $(i_1,i_2\ll R_{\rm H}/a_1)$ only affect the results at earlier times. The long-term statistics of CEs for nearly coplanar systems is better

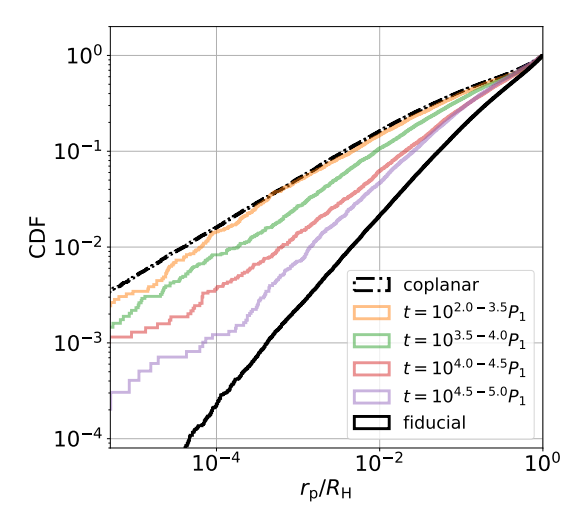


Figure 10. Same as Figure 4, showing the time evolution of the cumulative distribution of $r_{\rm p}$. The colored lines show the results for a system with initial inclination $i_1 = i_2 = 10^{-5} R_{\rm H}/a_1$, and different colors indicate different time intervals of the simulations. The black lines show the total distribution for the exact coplanar system (dash-dot) and the fiducial system (solid) for comparison.

represented by our fiducial simulations with $i_1 = i_2 = R_{\rm H}/a_1$ (see Section 3).

5. EFFECTS OF FRICTIONAL DISK FORCES

The AGN disk can affect the dynamical evolution of the embedded BHs. For example, a BH (with mass m_1 and semi-major axis a_1) experiences eccentricity damping on the timescale (Tanaka & Ward 2004)

$$\tau_e \simeq \frac{M^2 h^4}{2\pi m_1 \Sigma a_1^2} P_1$$

$$\simeq 1.2 \times 10^6 \left(\frac{a_1}{10^2 GM/c^2}\right)^{-2} \left(\frac{\Sigma}{10^5 \text{g/cm}^2}\right)^{-1}$$

$$\times \left(\frac{h}{0.03}\right)^4 \left(\frac{m_1}{10M_{\odot}}\right)^{-1} P_1, \tag{21}$$

where Σ is the disk surface density and h is the disk aspect ratio, and we have adopted some representative parameters for AGN disks (e.g., Sirko & Goodman 2003; see Figure 1 of Secunda et al. 2019). In the previous sections, we have studied BH binary captures via very close encounters in the absence of any disk force on the BHs. A full exploration of the effects of disk forces on BH binary formation would require long-term hydrodynamical simulations and is beyond the scope of this paper. Here, to qualitatively assess the effect of the disk, we apply simple prescriptions of disk forces on the BHs in our N-body simulations.

We consider two simple models for the disk forces:

1. The first model includes the frictional force (per unit mass):

$$F_{\text{drag}} = -\frac{v - v_{\text{K}}}{\tau_{\text{drag}}},$$
 (22)

where $\mathbf{v}_{\mathrm{K}} = \sqrt{GM/r^3} \; \hat{\theta}$ is the Keplerian velocity and r is the instantaneous distance of the BH to the SMBH. This force tends to damp the BH velocity \mathbf{v} to \mathbf{v}_{K} and damp its eccentricity around the SMBH at the rate $\dot{e} \simeq -e/\tau_{\mathrm{drag}}$.

2. The second model includes a force that mimics a migration trap at radius r_0 :

$$\boldsymbol{F}_{\text{trap}} = -\frac{\Omega_{\text{K},0}(r - r_0)}{\tau_{\text{trap}}} \hat{\boldsymbol{\theta}}, \qquad (23)$$

where $\Omega_{\mathrm{K},0} = \sqrt{GM/r_0^3}$ is the Keplerian frequency at r_0 . Equation (23) assumes that the torque on the BH at r is approximately linear in $(r-r_0)$ near the trap. In the following, we set r_0 to a_1 , the initial semi-major axis of m_1 .

The constants τ_{drag} and τ_{trap} in Equations (22) to (23) characterize the strengths of the disk forces. We apply these disk forces to our fiducial systems (see Section 3), considering different values of τ_{drag} and τ_{trap} . For each value case, we perform 200 simulations up to 10^5 orbit.

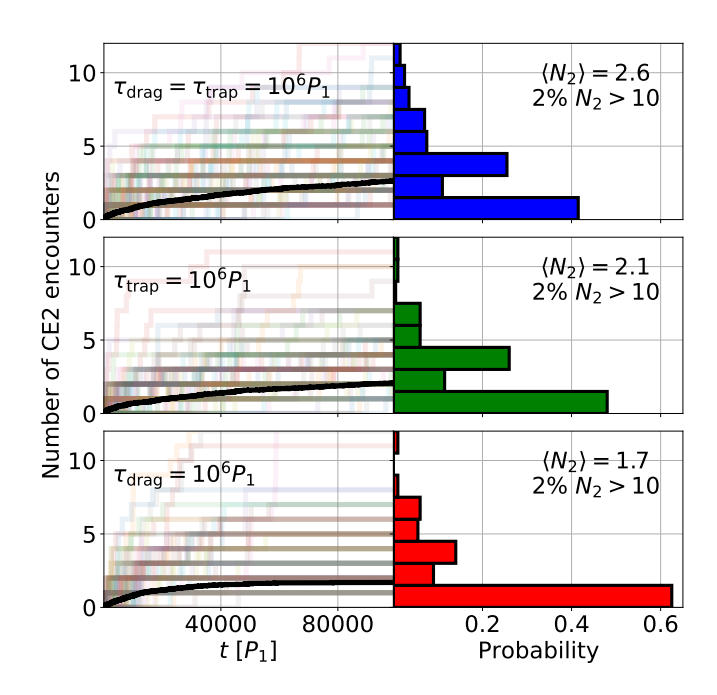


Figure 11. Similar to Figure 6, but for the fiducial systems (see Figure 1) and including the effects of disk forces. The type and the strength (timescale) of the adopted disk force for each panel is as labeled.

Figure 11 presents three example simulations: $\boldsymbol{F}_{\text{drag}}$ only with $\tau_{\text{drag}} = 10^6 P_1$, $\boldsymbol{F}_{\text{trap}}$ only with $\tau_{\text{trap}} = 10^6 P_1$, and both $\boldsymbol{F}_{\text{drag}}$ and $\boldsymbol{F}_{\text{trap}}$ with $\tau_{\text{drag}} = \tau_{\text{trap}} = 10^6 P_1$. The left panel shows the time evolution of N_2 and the right panel shows distribution of N_2 at $t = 10^5 P_1$. In all three cases, we have the average $\langle N_2(t=10^5 P_1)\rangle \simeq 2$. Due to the stochastic nature of the evolution, all three simulations exhibit large variation in the individual N_2 , with about 2% of the runs having $N_2(t=10^5 P_1) \gtrsim 10$.

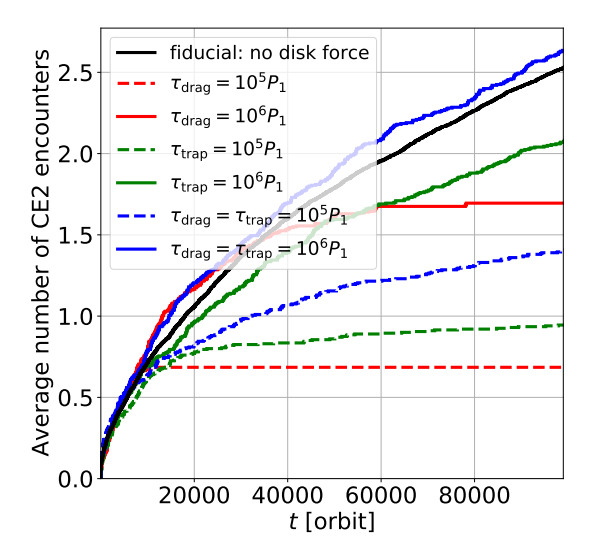


Figure 12. Average number of CE2 events as a function of the time in the fiducial systems (see Fig. 1), including different types and strengths of disk forces. For example, the red solid line refers to the case that includes only $\boldsymbol{F}_{\text{drag}}$ (with $\tau_{\text{drag}} = 10^6 P_1$), the green solid line includes only $\boldsymbol{F}_{\text{trap}}$ (with $\tau_{\text{trap}} = 10^6 P_1$), and the blue solid line includes both $\boldsymbol{F}_{\text{drag}}$ and $\boldsymbol{F}_{\text{trap}}$ (with $\tau_{\text{drag}} = \tau_{\text{trap}} = 10^6 P_1$).

Figure 12 shows the effects of different disk forces on the CE2 rates by comparing the time evolution $\langle N_2(t) \rangle$ from our simulations with different force types and strengths. The drag force (Equation 22) tends to stabilize the system by preventing crossing orbits between the BHs. When F_{drag} with $\tau_{\text{drag}} = 10^5 P_1$ (dashed red) or $10^6 P_1$ (solid red) is applied, the system is still unstable initially and the two BHs experience CE2 events (also see Li, Rodet and Lai, in prep). However, no more CE2s are found after about $t = 10^4 P_1$ for $\tau_{\text{drag}} = 10^5 P_1$ and $t = 8 \times 10^4 P_1$ for $\tau_{\text{drag}} = 10^6 P_1$. To check why CEs cease, Figure 13 compares the orbital separation of the two BHs in the no-drag simulations (fiducial, left panel) and the with-drag simulations ($\tau_{\rm drag} = 10^5 P_1$, right panel) at $t = 4 \times 10^3 P_1$, $1.2 \times 10^4 P_1$, and $2 \times 10^4 P_1$. In the fiducial simulations, $r_{\rm in} = a_{\rm in}(1 + e_{\rm in})$ (the apocenter distance of the inner BH to the SMBH) and $r_{\text{out}} = a_{\text{out}}(1-e_{\text{out}})$ (the pericenter distance of the outer BH) spread to the region with

 $r_{\rm out}-r_{\rm in}\lesssim 2.5R_{\rm H12}$ during the first 4000 orbits and remain in the same region at later time. This allows the two BHs to continue to "engage" with each other. However, in the $\tau_{\rm drag}=10^5P_1$ simulations, the BH orbits evolve in time toward smaller $r_{\rm in}$ and larger $r_{\rm out}$. Eventually, the difference between $r_{\rm out}$ and $r_{\rm in}$ becomes too large and CE becomes very rare. As a result, no CE2 happens between $t=2\times 10^4P_1$ and 10^5P_1 in the with-drag simulations.

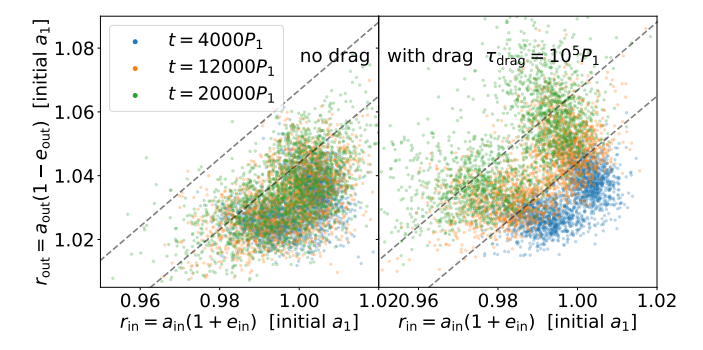


Figure 13. Apocenter of the inner BH $r_{\rm in} = a_{\rm in}(1 + e_{\rm in})$ and the pericenter of the outer BH $r_{\rm out} = a_{\rm out}(1 - e_{\rm out})$ from the fiducial (left) and the $\tau_{\rm drag} = 10^5 P_1$ simulations (right) at three different times. The region between the dashed lines corresponds to where $(r_{\rm out} - r_{\rm in})/R_{\rm H12} \in (2,3)$, with $R_{\rm H12}$ given by Equation (2) and assuming $a_{1,2} \simeq r_{\rm in,out}$. It is marked in both panels to help comparing the distributions.

One may expect that the trapping force (Equation 23) can accelerate the CEs by keeping the BH orbits close to the trapping radius. Our simulations show that when $\boldsymbol{F}_{\text{trap}}$ is applied, our systems indeed have more CE0 events. However, Figure 12 shows that the CE2 rate is actually smaller than the fiducial simulations without $\boldsymbol{F}_{\text{trap}}$: The average number of CE2 events becomes 2.1 for $\tau_{\text{trap}} = 10^6 P_1$ (solid green) and 0.9 for $\tau_{\text{trap}} = 10^5 P_1$ (dashed green) after 10^5 orbits. Unlike in the simulations with $\boldsymbol{F}_{\text{drag}} \neq 0$, the CE2 rate in our $\boldsymbol{F}_{\text{trap}} \neq 0$ simulations do not drop to zero at later times.

The stabilizing effects of the drag force and the trapping force can balance each other. The blue curves in Figure 12 show that applying $\tau_{\rm drag} = \tau_{\rm trap} = 10^5 P_1$ produces more CE2 events than applying either of the two forces. With $\tau_{\rm drag} = \tau_{\rm trap} = 10^6 P_1$, the two BHs experience slightly more CE2 events than in the fiducial simulations (black curve).

Figure 14 shows that the $r_{\rm p}$ -distributions of our simulations with drag forces are similar to the fiducial result. In particular, for $r_{\rm p}/R_{\rm H}\lesssim 0.01$, the linear scaling of the distribution with $r_{\rm p}$ remains accurate in all cases. In the simulations with the trap force, the mild encounters with $r_{\rm p}/R_{\rm H}\gtrsim 0.01$ are relatively more frequent than in the fiducial system with no disk forces (as the CDFs

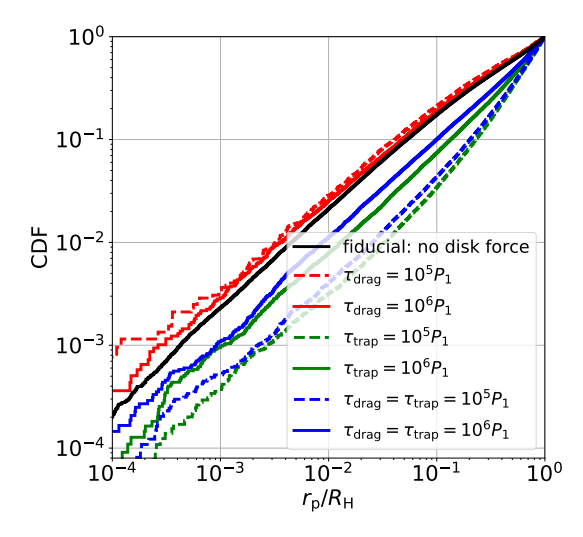


Figure 14. Similar to Figure 3, but showing the cumulative distribution of r_p in CE0 events for systems with different types and strengths of disk forces.

with the trap force have a larger slope at $r_{\rm p}/R_{\rm H} \gtrsim 0.01$). Thus the simple power-low distribution of $r_{\rm p}$ given by Equation (14) is still valid for CE2 but becomes less accurate for CE0 when $F_{\rm trap}$ is applied.

In a real AGN disk, multiple effects can take place at the same time. The outcome of their competition depends on the detailed disk properties. Our results in this section suggest that disk forces have little effect on the $r_{\rm p}$ -distribution for very close encounters (Figure 14), but can influence the CE2 event rate (Figure 12), and therefore affecting the BBH formation rate. Our simulations also suggest that in order for the two unstable BHs in a AGN disk to capture into a merging binary, a combination of the drag force and trapping force from the disk is needed, or we would rely on the chance that an individual system is in the high- N_2 tail of the distribution. We emphasize that our results in this section are based on simple prescriptions of disk forces. Hydrodynamics simulations will be needed to fully capture the effects of disk forces.

6. THREE AND MORE BHs AROUND SMBH

While a "SMBH + 2BHs" system is unstable only if $a_2 - a_1 \lesssim 2\sqrt{3}R_{\rm H}$ (see Equation 1), no precise stability criterion exists for systems with more than two BHs. In fact, such systems always exhibit instability eventually, except that the instability time grows with increasing orbital spacings. Numerical integrations suggest that a system of 3 or more bodies on nearly circular, coplanar orbits around a central massive object is stable for at least N orbital periods if the separation between adjacent bodies satisfies $|a_{j+1} - a_j| \gtrsim K(N)R_{\rm H}$, where

the constant K(N) increases with increasing N (e.g., $K \simeq 9 - 12$ for $N = 10^{10}$; Smith & Lissauer 2009).

To explore close encounters in systems with more than two BHs, we consider a "SMBH + 3BHs" system with $(m_1, m_2, m_3) = (2, 1, 0.5) \times 10^{-5} M$ and a "SMBH + 5 BHs" system with $(m_1, m_2, m_3, m_4, m_5) = (2, 1, 0.5, 0.25, 0.125) \times 10^{-5} M$, where M is mass of the central SMBH. The initial orbital separation is set as

$$a_{j+1} - a_j = KR_{H,\text{mut}}, \tag{24}$$

where $R_{\rm H,mut}$ is mutual Hill radius of m_j and m_{j+1} (see Equation 2) and we set K=2 or 4. The BHs are given initial eccentricities $e_1=0,\ e_j=10^{-5}$ for j>1 and inclinations $i=R_{\rm H}/a_1$ for all BHs. Similar to our fiducial simulations (Section 3), we carry out 2000 runs and sample the initial values of the argument of the peripasis, the longitude of the ascending node, and the mean anomaly randomly in the range $[0,2\pi]$ for each BH, assuming they all have uniform distributions.

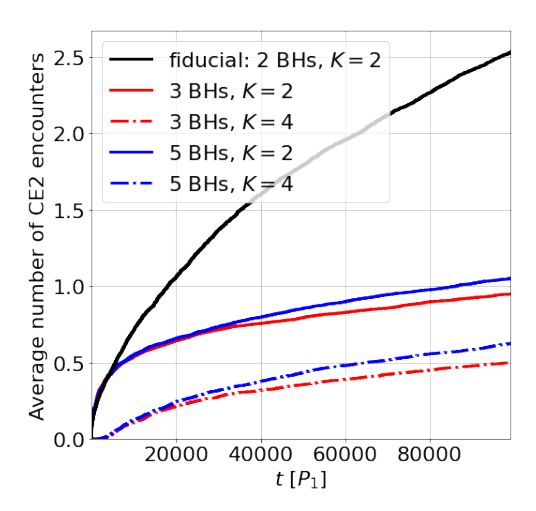


Figure 15. Average number of CE2 as a function of time for systems with 3 and 5 BHs. The fiducial result for 2 BHs (the bottom left planel of Figure 1) is also shown for comparison.

Figure 15 shows the averaged cumulative CE2 rates for systems with two, three and five BHs. The two-BH (fiducial) systems experience nearly 3 to 5 times more CE2 events than the other systems. For the K=2 cases, the average number of CE2 events at $t=10^5P_1$ is 0.9 with 3 BHs and 1.1 with 5 BHs. The fact that the CE2 rate is highest for the two-BH systems is somewhat surprising. It may be because the two-BH systems are subjected to conservation constraints, which cause the BH orbits to repeatedly overlap. A three-or-more-BH architecture has more degrees of freedom and there is no conservation law between any two BHs.

Adopting K=4 in the three- and five-BH simulations leads to no CE2 events before $t \simeq 2 \times 10^3 P_1$. This is be-

cause the initial conditions with larger K require longer times for the BHs to develop their first Hill sphere crossing. After the instability develops, the K=4 systems catch up in the growth rate. At $t=10^5P_1$, the three-BH and five-BH simulations with K=4 yield $\langle N_2 \rangle = 0.5$ and 0.62, respectively. For systems with larger K, we expect a longer time before the CEs occur, but the CE rate will eventually converge.

We fit the time evolution of the average number of CE2 events for $t > 5 \times 10^4 P_1$, by

$$\langle N_2(t)\rangle = \left(\frac{t}{T}\right)^{n_2}.$$
 (25)

Least-square fit gives $n_2 = 0.26$, 0.50, 0.30, 0.50 and $T = 1.2 \times 10^5$, 4.0×10^5 , 8.5×10^4 , 2.6×10^5 for 3 BHs with K = 2, 3 BHs with K = 4, 5 BHs with K = 2 and 5 BHs with K = 4, respectively. Using $\langle N(t; r_p < r_{\rm cap}) \rangle = \langle N_2(t) \rangle P_2(< r_{\rm cap})$ (see Equation 16) with $P_2(< r_{\rm cap}) \simeq r_p/(10^{-2}R_{\rm H})$ (see Equation 14), we find that it would take about $5 \times 10^{12}P_1$, 4×10^9P_1 , $4 \times 10^{11}P_1$, 3×10^9P_1 on average to form a merging BH binary in each of the four cases.

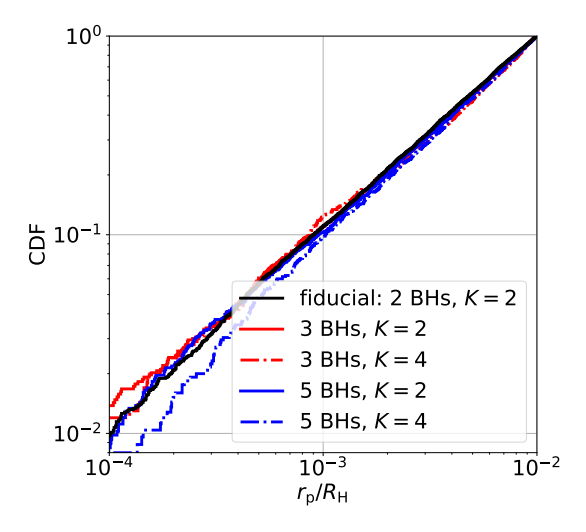


Figure 16. Same as Figure 3, except showing the cumulative distribution of $r_{\rm p}$ in close encounters (CE2 only) in simulations with different number of BHs and initial spacings.

Figure 16 shows that the $r_{\rm p}$ -distributions of CE2 for all of the simulations in this section are similar to the fiducial result (see Figure 3). Figure 17 shows that CE2 always have nearly uniform distributions of $\cos i_{\rm bin}$ and thus the merging BH binaries formed in our scenario have a wide range of inclination angles with respect to the AGN disk plane. This is expected: Regardless of the number and the initial spacings of the BHs, the relative orbit of the captured binary is dominated by the

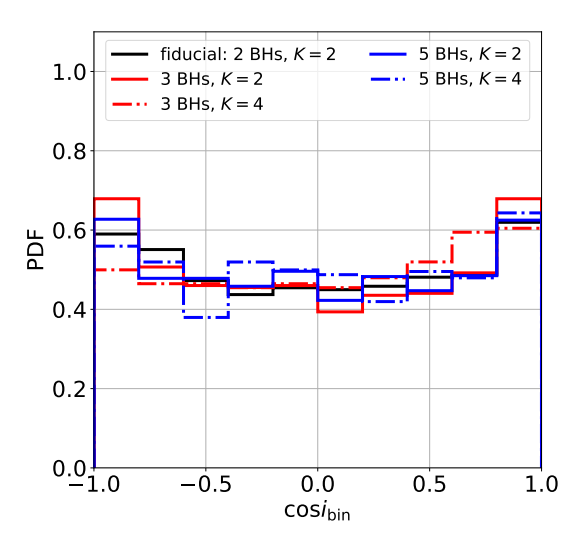


Figure 17. Same as Figure 5, except showing the results for the CE2 events in the simulations with different number of BHs and initial spacings.

gravity of the BHs during the CEs. Having more BHs and different initial spacings only affects the CE rate.

7. SUMMARY AND DISCUSSION

In this paper, we have studied the long-term evolution of two or more stellar-mass BHs on closely-packed, dynamically unstable circular orbits around a SMBH, with the initial semi-major axes separated by a few times the Hill radius $R_{\rm H}$. Such an orbital configuration may naturally arise from BH migrations in the AGN disk and leads to recurring close encounters between the BHs. We use N-body simulations to study the statistics and rate of close encounters (of various degrees of "closeness" compared to $R_{\rm H}$), the properties of the relative orbits of the encountering BHs, and the probability for two BHs to be captured into a merging binary with the help of gravitational wave emission during very close encounters. Our fiducial simulations focus on "SMBH + 2 BHs" systems with $m_1 = 2m_2 = 2 \times 10^{-5} M$ and initial inclinations $i_1 = i_2 = R_{\rm H}/a_1$ (where a_1 and a_2 are the BHs' semi-major axes around the SMBH). Additions simulations with different BH masses, initial orbital inclinations, prescriptions for disk forces, and different number of BHs are also performed.

Our simulations show that close encounters (CEs) between the BHs in such systems exhibit three general characteristics:

1. Close encounters (with the separation between two BHs less than $R_{\rm H}$) occur stocastically and the rate of CEs generally declines in time (see Fig. 1). The average cumulative number of CEs, $\langle N(t) \rangle$, is approximately a power-law function of time, although there are wide spreads in N(t) for different

- systems. For our fiducial "SMBH + 2 BHs" setup, we find $\langle N(t) \rangle \propto t^{0.5}$ (see Eqs. 9-11).
- 2. The vast majority of the CEs result in the formation of short-lived binaries with a small binding energy (of order $Gm_1m_2/R_{\rm H}$; see Fig. 2). Such binaries are quickly destroyed by the SMBH tide and do not lead to binary mergers.
- 3. The closest separation $(r_{\rm p})$ during a close encounter follows a cumulative distribution $P(< r_{\rm p}) \propto r_{\rm p}$ for $r_{\rm p} \ll R_{\rm H}$ (see Figs. 3, 4, and Eq. 14). This distribution is robust, regardless of the BH masses (Section 3.5) and the number of BHs in the system (Section 6). For systems with very small but non-zero initial mutual inclinations, the same $r_{\rm p}$ -distribution applies at later times as the mutual inclinations grow. In a system with two exact co-planar BHs, the distribution becomes $P(< r_{\rm p}) \propto r_{\rm p}^{1/2}$ (Fig. 8 and Eq. 19).

These results imply that, to capture an encountering BH pairs into a "permenant" binary, a fast dissipative mechanism is required. Given the high close encounter rate, a promising mechanism is the GW emission when $r_{\rm p}$ is very small (less than the critical "capture" radius $r_{\rm cap} \sim 10^{-4} R_{\rm H}$, depending on the system parameters; see Eq. 6):

- 4. We provide a semi-analytical formula for the averaged cumulative rate of binary captures via GW emission in a "SMBH + 2 BHs" fiducial system, Equation (16) or (17), which is the product of the close encounter rate $\langle N(t) \rangle$ and the capture probability $P(< r_{\rm cap})$ during each encounter.
- 5. Our formula suggests that, in the fiducial systems, the timescale for two BHs to be captured is $10^8 P_1$ on average (assuming $r_{\rm cap} = 10^{-4} R_{\rm H}$) and $\lesssim 10^7 P_1$ for the 5% of the systems with $N(t) \gtrsim 4 \langle N(t) \rangle$. In the exact co-planar systems, the capture rate is much higher (see Eq. 20), and we find that the average binary capture time is $6 \times 10^3 P_1$.
- 6. After the two BHs are captured, we expect these BH binaries to merge in a few binary orbits. Their mergers will exhibit high eccentricities (see below) when entering the LIGO band (≥ 10 Hz) and will have a board distribution of orbital inclinations relative to the original AGN disk (see Figure 5).

We have carried out additional simulations to assess how the above results may be influenced by various system parameters and by the gas disk effects:

- 7. The masses of the BHs (relative to the mass of the SMBH) affect the close encounter rate only in a modest way (Section 3.5). For example, the rate of CEs with $r_{\rm p} \leq 10^{-2} R_{\rm H}$ decreases by a factor of ~ 2 when the BH masses are lowered by a factor of ten (see Figure 6). The $r_{\rm p}$ -distribution (Eq. 14) is robust. Thus, we expect that our fiducial binary capture rate, Equation (17), remain valid for systems with different BH masses.
- 8. The most optimal setup to get more binary captures in our scenario is with two exact co-planar BHs (see points 3 and 5 above). Such an exact co-planar system would have a higher rate of close encounters (see Fig. 7 and Eq. 18) and a flatter $r_{\rm p}$ -distribution (Fig. 8 and Eq. 19), leading to a greatly enhanced binary capture rate (Eq. 20). However, if the mutual inclination between the BH orbits is initially small but non-zero, it will inevitably grow and evolve to an "equilibrium" value $\sim R_{\rm H}/a_1$ (see Fig. 9), causing $P(< r_{\rm p})$ to converge to the fiducial result (see Fig. 10).
- 9. We have explored the effects of gas disks by applying simple prescriptions of disk forces (see Eqs. 22 and 23) on the BHs in our N-body simulations. We find that such prescribed disk forces do not necessarily lead to an enhanced binary capture rate. In fact, simple gas drags on the BHs may stop close encounters at late times. A "migration trap" force can sometimes balance the drag force and maintain the close encounter rate (see Fig. 12).
- 10. The number of BHs and their initial spacings in a closely-packed system do not affect the $r_{\rm p}$ -distribution (Fig. 16) and the orbital obliquity distribution (Fig. 17) during the very close encounters. We find that systems with more than 2 BHs have a lower close encounter rate than systems with two BHs.

Regarding point 6 above: Using Equation (6) for r_{cap} , we find that the GW emitted by the BH binary at capture has a frequency

$$f_{\text{cap}} = \frac{1}{\pi} \left(\frac{Gm_{12}}{r_{\text{cap}}^3} \right)^{1/2}$$

$$= (1.4 \,\text{Hz}) \,\eta^{3/7} \left(\frac{4\mu}{m_{12}} \right)^{-3/7} \left(\frac{a_{12}}{100GM/c^2} \right)^{-3/7}$$

$$\times \left(\frac{M}{10^8 M_{\odot}} \right)^{-2/7} \left(\frac{m_{12}}{100M_{\odot}} \right)^{-5/7} . \tag{26}$$

For the adopted parameter values, this frequency lies slightly below the LIGO band. Such a newly captured binary will merge within a few binary orbits. Using the standard gravitational radiation formulae (Peters 1964), it is easy to see that when the frequency of the GWs from the binary enters the LIGO band ($\gtrsim 10$ Hz), the binary can retain a very significant ($\gtrsim 0.5$) eccentricity.

The event rate of binary BH mergers produced in our scenario depends on the population of BHs in AGN disks, which is very uncertain. Nevertheless, given the binary capture timescale obtained in this paper, a nonnegligible event rate for such BH mergers may be expected. Perhaps the recently claimed eccentric merger event GW190521 (Gayathri et al. 2022) is an example.

The most uncertain aspects of the present study concern the effects of gas disks. Our conclusion on the gas effects (point 9 above) should be considered tentative. For future work, hydrodynamics simulations should be used for a more in-depth study of the disk effects. Although we have only considered GW emission in this paper, the broad range of $r_{\rm p}$ in close encounters may allow

the physical processes at different distance scales to operate. For example, interaction between the circum-BH disks may generate dissipation for the BH pairs during close encounters. Our results of the close encounter rate and the $r_{\rm p}$ -distribution can be applied to these alternative dissipation mechanisms to explore different possibilities of binary BH formation in AGN disks.

ACKNOWLEDGMENTS

This work is supported in by NSF grant AST-2107796 and the NASA grant 80NSSC19K0444.

Software: Rebound (Rein & Liu 2012), Matplotlib (Hunter 2007), NumPy (van der Walt et al. 2011), SciPy (Virtanen et al. 2020)

REFERENCES

Abbott, B. P., Abbott, R., Abbott, T. D., et al. 2019, ApJL, 882, L24

Abbott, R., Abbott, T. D., Abraham, S., et al. 2021, ApJL, 913, L7

Antonini, F., & Perets, H. B. 2012, ApJ, 757, 27

Banerjee, S., Baumgardt, H., & Kroupa, P. 2010, MNRAS, 402, 371

Bartos, I., Kocsis, B., Haiman, Z., & Márka, S. 2017, ApJ, 835, 165

Baruteau, C., Cuadra, J., & Lin, D. N. C. 2011, ApJ, 726, 28

Belczynski, K., Bulik, T., Fryer, C. L., et al. 2010, ApJ, 714, 1217

Belczynski, K., Holz, D. E., Bulik, T., & O'Shaughnessy, R. 2016, Nature, 534, 512

Bellovary, J. M., Mac Low, M.-M., McKernan, B., & Ford, K. E. S. 2016, ApJL, 819, L17

Downing, J. M. B., Benacquista, M. J., Giersz, M., & Spurzem, R. 2010, MNRAS, 407, 1946

Ford, K. E. S., & McKernan, B. 2021, arXiv e-prints, arXiv:2109.03212

Fragione, G., & Kocsis, B. 2019, MNRAS, 486, 4781

Gayathri, V., Healy, J., Lange, J., et al. 2022, Nature Astronomy

Gladman, B. 1993, Icarus, 106, 247

Graham, M. J., Ford, K. E. S., McKernan, B., et al. 2020, PhRvL, 124, 251102 Gröbner, M., Ishibashi, W., Tiwari, S., Haney, M., & Jetzer, P. 2020, A&A, 638, A119

Hamers, A. S., Bar-Or, B., Petrovich, C., & Antonini, F. 2018, ApJ, 865, 2

Hunter, J. D. 2007, Computing in Science and Engineering, 9, 90

Ishibashi, W., & Gröbner, M. 2020, A&A, 639, A108

Kremer, K., Chatterjee, S., Ye, C. S., Rodriguez, C. L., & Rasio, F. A. 2019, ApJ, 871, 38

Leigh, N. W. C., Geller, A. M., McKernan, B., et al. 2018, MNRAS, 474, 5672

Li, J., & Lai, D. 2020, ApJL, 898, L20

Li, R., & Lai, D. 2022, arXiv e-prints, arXiv:2202.07633

Li, Y.-P., Dempsey, A. M., Li, H., Li, S., & Li, J. 2021a, arXiv e-prints, arXiv:2112.11057

Li, Y.-P., Dempsey, A. M., Li, S., Li, H., & Li, J. 2021b, ApJ, 911, 124

Lipunov, V. M., Postnov, K. A., & Prokhorov, M. E. 1997, Astronomy Letters, 23, 492

Liu, B., & Lai, D. 2018, ApJ, 863, 68

—. 2019, MNRAS, 483, 4060

—. 2021, MNRAS, 502, 2049

Liu, B., Lai, D., & Wang, Y.-H. 2019a, ApJ, 881, 41

—. 2019b, ApJL, 883, L7

Mandel, I., & de Mink, S. E. 2016, MNRAS, 458, 2634

Marchant, P., Langer, N., Podsiadlowski, P., Tauris, T. M., & Moriya, T. J. 2016, A&A, 588, A50

- McKernan, B., Ford, K. E. S., Kocsis, B., Lyra, W., & Winter, L. M. 2014, MNRAS, 441, 900
- McKernan, B., Ford, K. E. S., Lyra, W., & Perets, H. B. 2012, MNRAS, 425, 460
- McKernan, B., Ford, K. E. S., Bellovary, J., et al. 2018, ApJ, 866, 66
- McKernan, B., Ford, K. E. S., Bartos, I., et al. 2019, ApJL, 884, L50
- Miller, M. C., & Hamilton, D. P. 2002, ApJ, 576, 894
- Miller, M. C., & Lauburg, V. M. 2009, ApJ, 692, 917
- O'Leary, R. M., Rasio, F. A., Fregeau, J. M., Ivanova, N., & O'Shaughnessy, R. 2006, ApJ, 637, 937
- Peters, P. C. 1964, Physical Review, 136, 1224
- Petrovich, C., & Antonini, F. 2017, ApJ, 846, 146
- Podsiadlowski, P., Rappaport, S., & Han, Z. 2003, MNRAS, 341, 385
- Portegies Zwart, S. F., & McMillan, S. L. W. 2000, ApJL, 528, L17
- Pu, B., & Lai, D. 2021, MNRAS, 508, 597
- Quinlan, G. D., & Shapiro, S. L. 1989, ApJ, 343, 725
- Rein, H., & Liu, S. F. 2012, A&A, 537, A128
- Rein, H., & Spiegel, D. S. 2015, MNRAS, 446, 1424
- Rodriguez, C. L., Morscher, M., Pattabiraman, B., et al. 2015, PhRvL, 115, 051101
- Samsing, J., & D'Orazio, D. J. 2018, MNRAS, 481, 5445
- Samsing, J., MacLeod, M., & Ramirez-Ruiz, E. 2014, ApJ, 784, 71
- Samsing, J., Bartos, I., D'Orazio, D. J., et al. 2020, arXiv e-prints, arXiv:2010.09765

- Secunda, A., Bellovary, J., Mac Low, M.-M., et al. 2019, ApJ, 878, 85
- -.. 2020, ApJ, 903, 133
- Silsbee, K., & Tremaine, S. 2017, ApJ, 836, 39
- Sirko, E., & Goodman, J. 2003, MNRAS, 341, 501
- Smith, A. W., & Lissauer, J. J. 2009, Icarus, 201, 381
- Stone, N. C., Metzger, B. D., & Haiman, Z. 2017, MNRAS, 464, 946
- Tagawa, H., Haiman, Z., Bartos, I., & Kocsis, B. 2020a, ApJ, 899, 26
- Tagawa, H., Haiman, Z., & Kocsis, B. 2020b, ApJ, 898, 25
- Tanaka, H., & Ward, W. R. 2004, ApJ, 602, 388
- The LIGO Scientific Collaboration, the Virgo Collaboration, Abbott, R., et al. 2021, arXiv e-prints, arXiv:2108.01045
- Thompson, T. A., Quataert, E., & Murray, N. 2005, ApJ, 630, 167
- van der Walt, S., Colbert, S. C., & Varoquaux, G. 2011, Computing in Science and Engineering, 13, 22
- VanLandingham, J. H., Miller, M. C., Hamilton, D. P., & Richardson, D. C. 2016, ApJ, 828, 77
- Virtanen, P., Gommers, R., Oliphant, T. E., et al. 2020, Nature Methods, 17, 261
- Yang, Y., Bartos, I., Haiman, Z., et al. 2019a, ApJ, 876, 122Yang, Y., Bartos, I., Gayathri, V., et al. 2019b, PhRvL, 123, 181101
- Ziosi, B. M., Mapelli, M., Branchesi, M., & Tormen, G. 2014, MNRAS, 441, 3703